COBEM 2023 27TH INTERNATIONAL CONGRESS OF MECHANICAL ENGENEERING

ABCM Brazilian Society of Mechanical Sciences and Engineering
27th ABCM International Congress of Mechanical Engineering
December 04-08, 2023, Florianópolis-SC, Brazil

COB-2023-1598
EXPERIMENTAL CHARACTERIZATION OF AUTOMOTIVE ETHANOL COMMERCIALLY AVAILABLE IN BRAZIL

Fabio Bongoski
Roberto Wolf Francisco Jr
State University of Santa Catarina – Joinville/SC - Brazil
fabio.b@edu.udesc.br
roberto.francisco@udesc.br

Abstract. *Petroleum-derived fuels are energy sources used worldwide, but current levels of consumption have negative consequences due to the power of environmental pollution. In this context, an alternative to the use of gasoline is bioethanol, a fuel that is attractive because it comes from a renewable source, favors sustainability and has a high octane value. Several aspects must be analyzed to characterize a fuel, in this work we approach the adiabatic laminar flame velocity, apparent global activation energy and higher heating value. These characteristics are defined by the physicochemical properties of the fuel, which depend on factors such as its composition, pressure, temperature and equivalence ratio. The objective of the present study is to characterize the ethanol fuel sold in Brazil, firstly in the analytical condition (anhydrous) with a minimum content of 99.3% of the ethanol mass, and later, an analysis of the automotive ethanol sold at gas stations. The greatest variation in the composition of the analyzed fuels is found in the amount of water, and it is possible to perceive that the adiabatic laminar flame velocity and the higher heating value of the automotive ethanol samples present significantly lower results, as well as the apparent global activation energy showing higher values when compared to the analytical fuel. These characteristics are fundamental for the design of combustion systems and the development of chemical kinetic mechanisms for the analysis and use of bioethanol.*

Keywords: *bioethanol, adiabatic laminar flame velocity, apparent global activation energy, flat flame.*

1. INTRODUCTION

In the fuel scenario, gasoline occupies a prominent position among the most consumed, and in 2022, according to The Global Economy magazine, global consumption was $2.31 \cdot 10^7$ thousand barrels per day of fuel (Valev et al., 2022). As gasoline is derived from petroleum, its excessive use reflects in large amounts of pollutants released into the atmosphere, in recent years we have observed climate changes resulting from global warming, due to the massive burning of petroleum-derived fuels, reflecting largely in the increase of gases greenhouse effect (Erec and Greenpeace, 2010). To reduce the negative effects imposed on the environment, the use of bioethanol as fuel or as a mixture for gasoline becomes attractive, as it can be manufactured from the fermentation of agricultural raw materials, such as sugar cane, corn, oats, barley, wheat, sorghum and other sources of organic material. In addition to the factors mentioned, it should be taken into account that, as it is a fuel from plant sources, part of the pollutants released into the atmosphere is recovered by the plant itself in the form of CO_2, resulting in a carbon cycle. (García Camús and García Laborda, 2012).

The Brazilian government determines through the Agencia Nacional do Petróleo, Gás Natural e Biocombustíveis (ANP) legislation to regulate ethanol production. This regulation is presented by ANP Resolution No. 907, of November 18, 2022 - DOU of 11-23-2022 (BRAZIL, 2022), which determines the production and quality specifications of ethanol in Brazil. Among the types of ethanol available, commercial anhydrous ethanol (CAE) and commercial hydrous ethanol (CHE) were selected for analysis in this work. Table 1 presents the characteristics required for the production of each selected ethanol.

Table 1 - Characteristics that must be present in the compliance bulletin issued by the distributor of liquid fuels.

FEATURE	UNIT	LIMIT	
		CAE	CHE
Aspect	-	Clear and free of impurities	
Total acidity, max. (Acetic Acid)	mg/L	30	
Electrical conductivity, max.	µS/m	300	
Density at 20 ºC	kg/m³	791.5 max.	805.2 a 811.2
Alcohol content	% mass	99.3 min.	92.5 a 94.6

Hydrogen Potential (pH)	-	-	6.0 a 8.0
Ethanol content, min.	% volume	98	94.5
Water content, max.	% mass	0.7	7.5
Residue by evaporation, max.	mg/100mL	5	
Hydrocarbon content, max.	% volume	3	
Chloride content, max.	mg/kg	1	
Sulphate content, max.	mg/kg	4	
Iron content, max.	mg/kg	5	
Sodium content, max.	mg/kg	2	
Copper content, max.	mg/kg	0.07	-
Methanol content, max.	% volume	0.5	

It is noticed that there is a maximum acceptable content of components present in the mixture, thus avoiding excessive variations in the properties of these fuels, such as the adiabatic laminar velocity of the flame and the higher heat value. Among the components present in commercial ethanol, water can be highlighted, as it has the highest concentration (7.5% by mass) in the fuel and, therefore, may have a greater influence on its physicochemical properties, when compared to pure ethanol. Furthermore, the composition of commercial automotive ethanol (CHE) can also be affected due to the transport and storage of the fuel at filling stations, thus changing the composition of water present in the mixture.

Therefore, the objective of the present study is to characterize anhydrous and automotive ethanol commercialized in Brazil, with regard to combustion properties. The characterization was conducted in a simplified way, considering that the mixture composition consists only of ethanol and water. The properties of interest are the adiabatic laminar flame velocity, the apparent global activation energy and the higher heat value.

Automotive ethanol (CHE) was obtained directly from 3 different filling stations. Anhydrous ethanol (CAE) was also selected as a comparison parameter, thus allowing to highlight the influence of the water concentration in the mixture. In addition, the adiabatic flame velocity of the CAE has already been evaluated over the years by other researchers, using different experimental methods, as shown in Table 2. Thus, allowing the validation of the experimental bench used in the present work.

Table 2 - Authors and parameters used to measure S_{L0}

Author	Year	Φ	Method*	Initial Temp of Reagents [K]
(Eckart et al., 2021)	2021	0.6 – 1.6	HF	363
(Garzón Lama et al., 2020)	2020	0.8 – 1.3	VC	358
(Van Treek et al., 2019)	2019	0.7 – 1.4	HF	358
(Katoch et al., 2018)	2018	0.7 – 1.3	DC	300, 358, 453, 600
(Aghsaee et al., 2015)	2015	0.7 – 1.5	VC	318, 358, 373, 473
(Sileghem et al., 2014)	2014	0.7 – 1.5	HF	298, 318, 328, 338, 358
(Dirrenberger et al., 2014)	2014	0.65 – 1.55	HF	298, 358, 398
(Konnov et al., 2011)	2011	0.65 – 1.55	HF	298, 308, 318, 328, 338, 348, 358
(Bradley et al., 2009)	2009	0.7 – 1.5	VC	300, 358, 393

**CV – Constant volume method, HF – Heat-flux method and DC – Diverging channel method.*

2. EXPERIMENTAL METHODOLOGY

2.1 DETERMINATION OF THE WATER CONCENTRATION IN THE FUEL

Initially, commercial fuels obtained from filling stations were evaluated in relation to the amount of water present in the samples. This procedure was necessary to allow the calculation of the air and fuel flows injected into the burner and to stabilize the flame in the stoichiometric condition.

The mass of water present in the samples obtained from the filling stations was determined by measuring the density of the mixture, using a 25 ml pycnometer and an analytical balance. The results were obtained by calculating the average of three measurements for each fuel sample.

Through Eq. (1), was possible to obtain the mole fraction of the chemical species (X_i) present in the fuel,

$$\rho_{mist} = \sum_i X_i \rho_i \tag{1}$$

where ρ_i is the density of chemical species *i*. Knowing X_i, through Eq. (2), the mass fraction (Y_i) of water and ethanol present in the fuel was determined,

$$Y_i = \frac{X_i\, MW_i}{MW_{mist}} \tag{2}$$

the term MW_i is the molar mass of each component and MW_{mist} is the molar mass of the mixture. Multiplying the result of the mass fraction of each component obtained in Eq. (2) by the total weight of the mixture, the amount of ethanol and water present in the fuel is obtained (Turns, 2013). CAE fuel was used as a reference, due to the ease of comparing the result with the literature.

2.2 EXPERIMENTAL BENCH

The adiabatic flame velocity and activation energy were measured experimentally using the flat flame method. Figure 1 presents the experimental diagram with the flat flame burner.

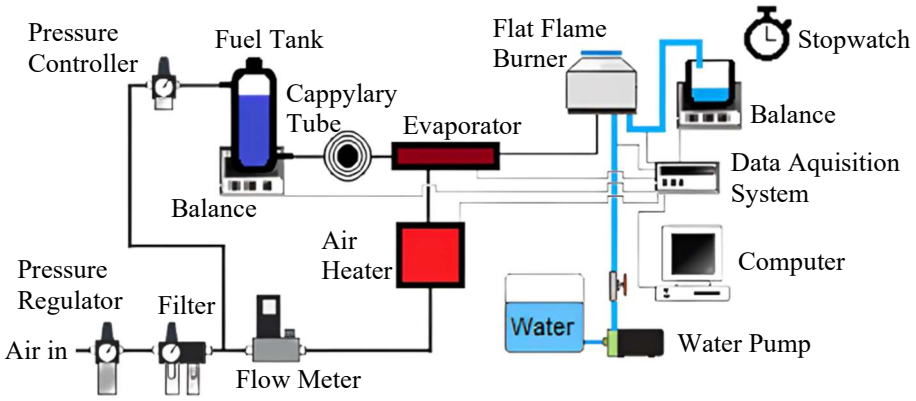

Figure 1 - Schematic diagram of the experimental configuration used in this work.

The air supply line consists of a pressure regulator adjusted to 5 bar, coalescing filter, flow controller (OMEGA FMA-2609A) and electric heater. The fuel supply line system consists of a pressurized fuel tank, a precision scale and an evaporator. The tank pressure is adjusted by means of a precision pressure regulator, according to the desired fuel flow. Air and fuel are premixed before being injected into the evaporator.

A precision balance (SHIMADZU UX4200H) was connected to the computer to measure the instant fuel mass in the tank over time. To control the temperatures, a data acquisition system (KEYSUGTH DAQ970A) and PT100 thermoresistors (MIT EXACTA TR) are placed in the air heater, evaporator, reagent inlet, water inlet and burner outlet. The cooling water originates in a reservoir, passes through a pump, then through the coil inside the porous plate and exits the burner. The mass flow rate of the cooling system water is determined by collecting the water several times in a container for a given time, then weighing it on a precision balance.

2.3 EXPERIMENTAL PROCEDURES

All tests were carried out with the reagents temperature of 358 K, atmospheric pressure and stoichiometric condition. The higher heat value was measured using an isoperibol calorimeter (Parr 6200).

The experimental study of adiabatic laminar flame velocity and overall activation energy was developed using the flat flame method and a commercial McKenna burner. The burner is made of a porous plate that includes a heat exchanger inside, both made of stainless metallic material. The assembly is synthesized to allow chemical bonds between the components (plate and tube). This procedure is necessary, as the heat exchange between the porous plate and the cooling water is essential for its operation.

To determine the adiabatic laminar flame velocity (S_{L0}), the heat transfer rate from the flame to the cooling system is measured for various non-adiabatic laminar flame velocity (S_L), for which it is possible to obtain a stable flat flame, maintaining the same equivalence ratio (Ø). The non-adiabatic laminar flame velocity injected into the burner is determined by measuring the volumetric flow rate of the reactants, using flow meters and the surface area of the burner.

Applying the global energy balance Eq. (3), the enthalpy of the products (h_p) and the reaction temperature (T_r) are calculated (Francisco and Oliveira, 2018).

$$\dot{m}_a h_a + \dot{m}_f h_f = \dot{m}_g h_p + q_{sw} \tag{3}$$

where ($\dot{m}_a$) is air mass flow, ($\dot{m}_f$) fuel mass flow, ($\dot{m}_g$) is the sum of the previous two, and (q_{sw}) heat transfer rate for cooling water.

Applying this concept at different flow rates, a table of flame temperature by non-adiabatic flame velocity S_L is obtained. It is worth noting that due to heat loss to the cooling system the measured flame velocity is lower than the adiabatic flame velocity. Then, using an asymptotic flame model Eq. (4) it is possible to obtain the relationship between the non-adiabatic laminar flame velocity S_L and the adiabatic laminar flame velocity S_{L0}, and also the value for apparent global activation energy,

$$ln\left(\frac{S_L}{S_{ref}}\left(\frac{T_{ro}}{T_r}\right)^{5/4}\right) = ln\left(\frac{S_{L0}}{S_{ref}}\right) + \frac{E_a}{2RT_{r0}}\left(1 - \frac{T_{ro}}{T_r}\right) \tag{4}$$

where (R) is the universal gas constant, (S_{ref}) is the reference value for adiabatic laminar flame velocity for the fuel used and serves to normalize the values of S_L. A redesign of the type $Y = b + mX$ can be applied to Eq. (4), to obtain the transformed variables X and Y,

$$Y = ln\left(\frac{S_L}{S_{ref}}\left(\frac{T_{ro}}{T_r}\right)^{5/4}\right) \text{ and } X = \left(1 - \frac{T_{ro}}{T_r}\right) \tag{5}$$

leaving the intercept b and slope m given by,

$$b = ln\left(\frac{S_{L0}}{S_{ref}}\right) \text{ and } m = \frac{E_a}{2RT_{r0}} \tag{6}$$

the model represents the fitted curve with the values of S_L and T_r. Thus, the adiabatic laminar flame velocity S_{L0} and the apparent global activation energy (E_a) are obtained by intercepting the graph and slope of the curve (Francisco and Oliveira, 2018).

3. RESULTS AND DISCUSSIONS

3.1 DENSITY AND HHV OF THE FUEL

Table 3 presents the measured values of the density, the ethanol concentration in % of mass and the HHV of the fuels used. It can be seen that the measured values of density for each sample of ethanol CHE and ethanol CAE are in accordance with the legislation presented in Table 1. Furthermore, the HHV measurement was repeated 3 times for each sample, with the maximum standard deviation being 97 kJ/kg.

With regard to the CHE samples, it can be observed that the measured values of the density and the HHV were very close, despite the samples having been obtained from different filling stations and different manufacturers. The lower HHV for CHE when compared to CAE is a result of the concentration of water present in the mixture.

Table 3 – Density, amount of ethanol and HHV for each fuel.

Fuel	ρ* [kg/m³]	σ	Ethanol [% m/m]	HHV [kJ/kg]	σ
CAE	790.4	0.24	99.82	29432	12.22
CHE 1	811.03	0.05	95.68	27381	97.07
CHE 2	811.13	0.08	95.66	27358	73.43
CHE 3	811.23	0.17	95.64	27291	90.46

**Fuel temperature to determine ρ equal to 293.15 K.*

3.2 DETERMINATION OF THE S_{LO} AND E_a

Figure 2 presents the values found in the literature over the years for S_{L0} of anhydrous ethanol (CAE) with the same conditions imposed in the present work, Ø = 1 and reagent temperature of 358 K, only the work of Eckart et al. (2021) has a reagent temperature of 363 K.

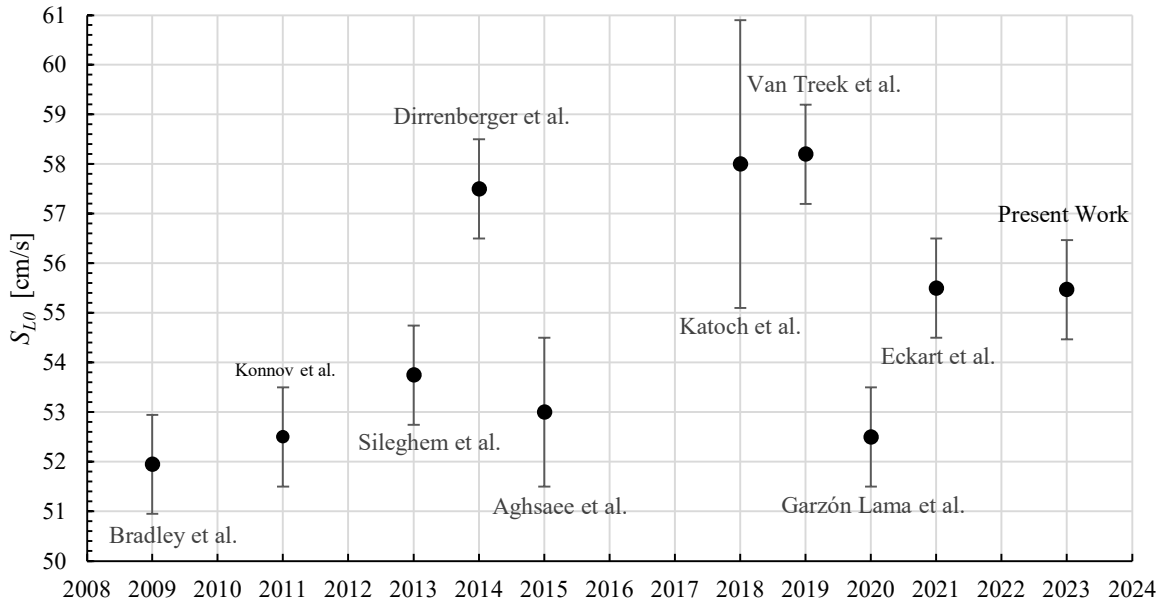

Figure 2 – Values of S_{L0} for anhydrous ethanol by different authors over the years.

It can be seen that for pure ethanol there is no convergence of experimental results within the analyzed period (2009 to 2023), which may hinder the development of chemical kinetic mechanisms for this fuel. The highest and lowest flame velocities measured were approximately 58.2 and 52 cm/s, respectively. However, the error bars presented by the authors suggest that the results could converge for velocities between 54 and 57 cm/s. Still, it can be observed that the measurement uncertainty of the flame velocity of the present work is close to the values presented by other authors, using different methods.

Figure 3 shows the curves of the transformed variables X and Y obtained experimentally for the CAE fuel and the three samples of the CHE fuel.

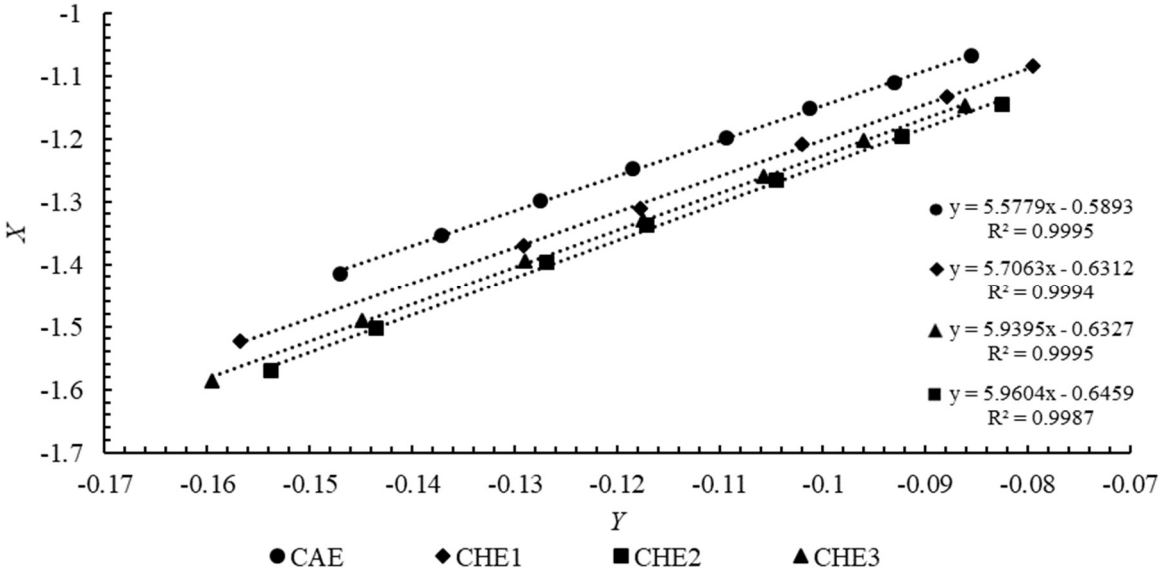

Figure 3 - Linear regression for each fuel dataset.

For each fuel, between 5 and 8 stability points were obtained, keeping constant the equivalence ratio and the reactant temperatures. For the 4 curves, the R2 factor was greater than 99.8%, indicating that the experimental points presented an excellent correlation with the equations of the curves.

Using the values of b and m obtained through linear regression applied to the dataset obtained experimentally for each fuel, it is possible to calculate the adiabatic laminar flame velocity and apparent global activation energy. Figure 4 presents the S_{L0} values in comparison with three chemical kinetic mechanisms, LNLL (Marinov, 1999), NUI Galway (Mittal et

al., 2014) end San Diego (Chemical-Kinetic Mechanisms for Combustion Applications, 2016), chosen because they include the chemical species C2H5OH (ethanol) in their reaction mechanism, necessary to describe the numerical results.

Numerical analysis was performed with the ANSYS CHEMKIN-PRO 2019 R3 software, applying the same conditions as the experiment, that is, reagent temperature of 358 K, ambient temperature of 296.15 K, Ø = 1 and P = 1 atm. The Gradient and Curvature parameters used were 0.01 and 0.01 and the grid limit was 5000 points.

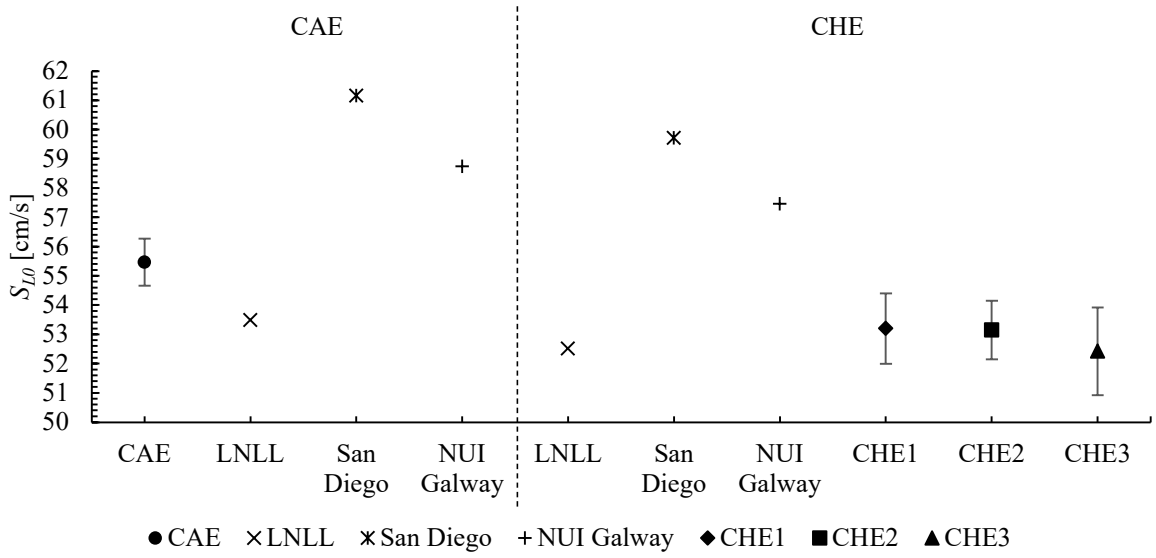

Figure 4 - Experimental and numerical S_{L0} for each fuel, T_{go} = 358 K, Ø = 1 and P = 1 atm.

The adiabatic flame velocity measured for the CAE was 55.47 cm/s. The addition of water resulted in an adiabatic flame velocity reduction of approximately 4 % for the 3 samples tested. Although commercial samples of hydrous ethanol were randomly obtained from different gas stations and different producers, the results for the adiabatic flame velocity were very close, with variations between 53.2 and 52.4 cm/s, representing less than 1.5 %.

Regarding the numerical and experimental results obtained for the CAE, it can be observed that the smallest percentage difference was 3.6%, using the LNLL mechanism. The San Diego mechanism showed a difference of 10 %. The same occurred with the CHE fuels, whose smallest difference obtained was 1.3 % for the LNLL mechanism. Thus, comparing the evaluated mechanisms, it is noticed that the LNLL showed greater agreement with the experiment for both types of fuel.

Another factor analyzed experimentally was the apparent global activation energy, which reflects the amount of initial energy required for the fuel to burn, the data are presented in Figure 5.

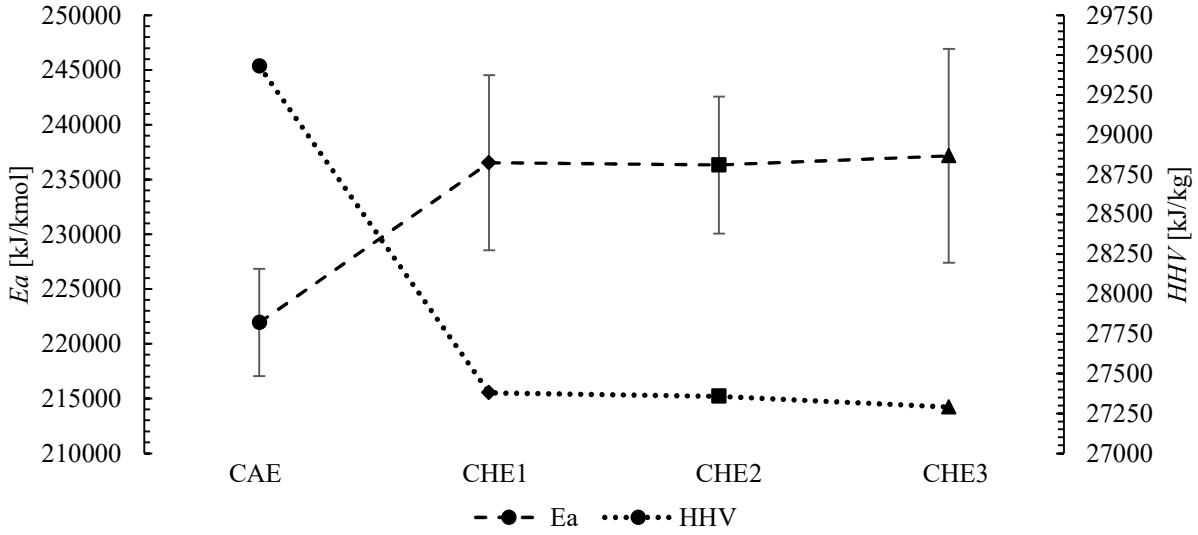

Figure 5 - Behavior of E_a and HHV factors.

The apparent global activation energy measured for CAE was 221949 kJ/kmol. The addition of water in the fuel resulted in a 6 % increase in E_a, considering all evaluated CHE fuel samples. It can also be seen that the three CHE samples showed very close E_a, despite the measurement uncertainty being approximately 4 %. The increase in activation energy with the addition of water is a result of the greater amount of energy required to initiate the combustion reaction.

In Figure 5 it can also be seen that the addition of water resulted in a 6% reduction in *HHV*. Among the CHE fuel samples, no significant *HHV* variation was observed.

4. CONCLUSIONS

An experimental study was conducted to characterize, in a simplified manner, two types of ethanol commercialized in Brazil. The experimental results for the density of the analyzed fuels comply with the regulations imposed by the ANP. The experimental result of the adiabatic laminar flame velocity for the CAE fuel is consistent with the values found in the literature, but significant variation was observed in the numerical study.

The comparison of the variation in the experimentally obtained adiabatic laminar flame velocity for the two types of analyzed fuels averaged 4.18%. The largest and smallest differences compared to the numerical models were 9.28% (San Diego) and 3.58% (LNLL) for the CAE fuel, and 10.98% (San Diego) and 1.20% (LNLL) for the CHE fuel. The apparent global activation energy of the CHE fuel showed an average increase of 6.42% compared to the CAE fuel, and the higher heating value (HHV) values for the CHE fuel exhibited a reduction of 7.27% compared to the CAE fuels, due to the higher concentration of water in the mixture.

5. ACKNOWLEDGEMENTS

The authors acknowledge the financial support of the Santa Catarina State Research and Innovation Foundation (FAPESC/Brazil - grant numbers 2021TR1321, 2021TR1457 and 2021TR843), National Council for Scientific and Technological Development (CNPq/Brazil - grant number 427885/2018-3) and Coordination for the Improvement of Higher Education Personnel (CAPES - Finance Code 001).

6. REFERENCES

Aghsaee, M., Nativel, D., Bozkurt, M., Fikri, M., Chaumeix, N., e Schulz, C. (2015) Experimental study of the kinetics of ethanol pyrolysis and oxidation behind reflected shock waves and in laminar flames. *Proceedings of the Combustion Institute*, *35*(1), 393–400. doi:10.1016/j.proci.2014.05.063

Bradley, D., Lawes, M., e Mansour, M. S. (2009) Explosion bomb measurements of ethanol-air laminar gaseous flame characteristics at pressures up to 1.4 MPa. *Combustion and Flame*, *156*(7), 1462–1470. doi:10.1016/j.combustflame.2009.02.007

BRAZIL. (2022) RESOLUÇÃO ANP Nº 907, DE 18 DE NOVEMBRO DE 2022 - DOU DE 23-11-2022. Obtained from: https://atosoficiais.com.br/anp/resolucao-n-907-2022.

Chemical-Kinetic Mechanisms for Combustion Applications (2016), San Diego Mechanism web page, Mechanical and Aerospace Engineering (Combustion Research), University of California at San Diego (http://combustion.ucsd.edu).

Dirrenberger, P., Glaude, P. A., Bounaceur, R., Le Gall, H., Da Cruz, A. P., Konnov, A. A., e Battin-Leclerc, F. (2014) Laminar burning velocity of gasolines with addition of ethanol. *Fuel*, *115*, 162–169. doi:10.1016/j.fuel.2013.07.015

Eckart, S., Fritsche, C., Krasselt, C., e Krause, H. (2021) Determining the laminar burning velocity of nitrogen diluted dimethoxymethane (OME1) using the heat-flux burner method: Numerical and experimental investigations. *International Journal of Energy Research*, *45*(2), 2824–2836. doi:10.1002/er.5978

Erec & Greenpeace. (2010) *Energy revolution: a sustainable world energy outlook, 3rd edition*.

Francisco, R. W., e Oliveira, A. A. M. (2018) Simultaneous measurement of the adiabatic flame velocity and overall activation energy using a flat flame burner and a flame asymptotic model. *Experimental Thermal and Fluid Science*, *90*(March 2017), 174–185. doi:10.1016/j.expthermflusci.2017.09.011

García Camús, J. M., e García Laborda, J. Á. (2012) Biocarburantes líquidos: Biodiesel y bioetanol. *Universidad Rey Juan Carlos del Círculo de Innovación en Tecnologías Medioambientales y Energía (CITME)*, *18*(1), 155–172.

Garzón Lama, L., Sotton, J., e Martins, C. A. (2020) Experimental burning velocities of ethanol-water-air at elevated pressure and temperature. *Fuel*, *265*(October 2019), 116933. doi:10.1016/j.fuel.2019.116933

Katoch, A., Millán-Merino, A., e Kumar, S. (2018) Measurement of laminar burning velocity of ethanol-air mixtures at elevated temperatures. *Fuel*, *231*(May), 37–44. doi:10.1016/j.fuel.2018.05.083

Konnov, A. A., Meuwissen, R. J., e De Goey, L. P. H. (2011) The temperature dependence of the laminar burning velocity of ethanol flames. *Proceedings of the Combustion Institute*, *33*(1), 1011–1019. doi:10.1016/j.proci.2010.06.143

Marinov, N. M. (1999) Kinetic Model for High Temperature Ethanol Oxidation. *Int. J. Chem. Kinet.*, *31*(3), 183–220.

Mittal, G., Burke, S. M., Davies, V. A., Parajuli, B., Metcalfe, W. K., e Curran, H. J. (2014) Autoignition of ethanol in a rapid compression machine. *Combustion and Flame*, *161*(5), 1164–1171. doi:10.1016/j.combustflame.2013.11.005

Sileghem, L., Alekseev, V. A., Vancoillie, J., Nilsson, E. J. K., Verhelst, S., e Konnov, A. A. (2014) Laminar burning velocities of primary reference fuels and simple alcohols. *Fuel*, *115*, 32–40. doi:10.1016/j.fuel.2013.07.004

Turns, S. R. (2013) *Introdução à combustão: conseitos e aplicações*.

Valev, N., Bieri, F., e Bizuneh, M. (2022) Gasoline consumption by country. *The Global Economy*. Obtido 3 de julho de 2023, de https://pt.theglobaleconomy.com/rankings/gasoline_consumption/

van Treek, L., Lubrano Lavadera, M., Seidel, L., Mauss, F., e Konnov, A. A. (2019) Experimental and modelling study of laminar burning velocity of aqueous ethanol. *Fuel*, *257*(August), 116069. doi:10.1016/j.fuel.2019.116069

7. RESPONSIBILITY NOTICE

The author(s) is (are) the only responsible for the printed material included in this paper.